Nuclear Engineering and Technology 52 (2020) 223–229

Contents lists available at ScienceDirect

Nuclear Engineering and Technology

journal homepage: www.elsevier.com/locate/net

Original Article

Reactor core analysis through the SP_3-ACMFD approach. Part I: Static solution

Morteza Khosravi Mirzaee*, A. Zolfaghari, A. Minuchehr

Faculty of Engineering, Shahid Beheshti University, P. O. Box: 1983963113, Tehran, I. R, Iran

ARTICLE INFO

Article history:
Received 24 December 2018
Received in revised form
16 June 2019
Accepted 24 July 2019
Available online 25 July 2019

Keywords:
Multi-dimensional multi-group neutron transport
Reactor core analysis
Simplified P_3 (SP_3) equations
ACMFD method
Static analysis

ABSTRACT

The present work proposes a solution to the static Boltzmann transport equation approximated by the simplified P_3 (SP_3) on angular, and the analytic coarse mesh finite difference (ACMFD) for spatial variables. Multi-group SP_3-ACMFD equations in 3D rectangular geometry are solved using the GMRES solution technique. As the core time dependent analysis necessitates the solution of an eigenvalue problem for an initial condition, this work is hence devoted to development and verification of the proposed static SP_3-ACMFD solver. A 3D multi-group static diffusion solver is also developed as a byproduct of this work to assess the improvement achieved using the SP_3 technique. Static results are then compared against transport benchmarks to assess the proximity of SP_3-ACMFD solutions to their full transport peers. Results prove that the approach can be considered as an acceptable interim approximation with outputs superior to the diffusion method, close to the transport results, and with the computational costs less than the full transport approach. The work would be further generalized to time dependent solutions in Part II.

1. Introduction

Accuracy of the neutron diffusion theory is not satisfactory for design and analysis of reactors with complex fuel assemblies e.g. MOX fueled LWRs [1]. Taking into account the rich phase space of transport equation, a time dependent analysis would be too expensive in the sense of computational cost. Among deterministic methods, *discrete ordinates* (S_N) or expansion through *spherical harmonics polynomials* (P_N) are the most favorable techniques to solve the transport equation. Although theoretical investigations predict a good convergence for large enough values of N, in practice it is not quite economic for core calculation [2]. To reduce the computational burden while saving the desired accuracy as much as possible, a number of efforts have focused on interim approaches which resulted in *Simplified* S_N (SS_N) as well as *Simplified* P_N (SP_N) for transport solutions [3–5]. These methods accompany the good precision of semi-analytic expansions alongside reducing the costs of computation through some acceptable simplifications for angular variables. The platform is therefore suitable for a time dependent analysis.

Based on analytic investigations [6], the SP_N approximation allocates less variables compared to its P_N counterpart. As an instance, a 3D even parity P_3 analysis requires six moments per node while the same analysis in SP_3 becomes possible with only two moments per node suggesting an incredible saving.

In recent years many researchers have benefited SP_3 equations for complicated cores. Bahabadi et al. [7] proposed a new analytic function expansion nodal (AFEN) method for solving SP_3 static equations which uses analytic basis functions to expand 3D flux. So, it might be encountered as a novel expansion nodal method. More recently, the SP_N coupled with the finite element method was used for pinwise homogenization with less computational cost [8].

A rather quick scan over the works carried out on the SP_3 approach decisively indicates a fast growth of interests in this plausible approximation. For instances, Chao [9] continues efforts on his proposed generalized SP_N (GSP_N) equations already developed for a generic case of multi-group anisotropic neutron source with improved boundary conditions [10,11]. Though Chao derived some new and complicated interface and boundary conditions plus more differential equations to improve the accuracy of original SP_N equations, the work is not yet supported by detailed numerical experiments to prove the predicted error reduction in applied problems. In another attempt, Cherezov et al. [12] focused on the diffusion and SP_3 equations for static 2D reactor core calculations

* Corresponding author.
E-mail addresses: mh_khosravi@sbu.ac.ir (M. Khosravi Mirzaee), A-zolfaghari@sbu.ac.ir (A. Zolfaghari), A.Minuchehr@sbu.ac.ir (A. Minuchehr).

https://doi.org/10.1016/j.net.2019.07.022

using the reduced order element method. At the same time, Zhang and Chen [13] tried to solve the SP_3 equations using the reduced basis finite element method. Meanwhile, the coupled diffusion/SP_3 method was implemented in a so called GLIM framework using the Hybrid Nodal Green's Function Method (HNGFM) [14]. Finally, Yang et al. [15] experienced the accelerated pin-by-pin calculations using the exponential function expansion nodal SP_3 solved by the GMRES technique applicable for PWRs.

At the time being, one can list many codes for static SP_3 solution but few with transient ability, topped by PARCS [16] and DYN3D [6]. Both codes benefit the nodal expansion method (NEM) for the spatial discretization. The code SCOPE2 is equipped with a semi-analytic nodal method for PWR core analysis [17]. We can also point to the SIMULATE-4 [18] wherein a variant of semi-analytic 2D SP_3-nodal formulation is coupled with an axial homogenization model to carry out 3D core calculations.

Analytic coarse mesh finite difference (ACMFD) method was first introduced by Chao [19] to derive an explicit analytic expressions for the two-group effective diffusion coefficients in both 3D Cartesian and hexagonal geometries. Later, Aragonés et al. [20] expanded the idea to multigroup case by transforming the physical nodal equations to the so-called mathematical *modal* space followed by solving energy decoupled equations there. The solutions are transformed back into the nodal space resulting in a coupled system of equations with group fluxes as unknowns.

In this paper we propose the extention of using ACMFD methodology for the solution of static SP_3 equations. A solver called SIMANOD is therefore developed based on the SP_3-ACMFD technique to carry out a number of static criticality calculations. To demonstrate the superiority of the adopted SP_3 technique over the diffusion outcome, we have also developed a difusion solver (DIFANOD) based on the ACMFD method. This way one will be able to keep the spatial approximation fixed for both codes and focus on the angular improvements achieved by the SP_3 kernel. Fianlly, to verify the code against transport results, a number of benchmarks are examined.

Here in Part I, static SP_3 equations in three dimensions are discussed, and satisfactory benchmarking which justify the superiority of new platform over the diffusion model is also proposed. This way, necessary initial conditions for transient problems can be generated through the solution of static eigenvalue equations solver. Then in Part II, the idea is generalized to time dependent equations where the numerical solution of transient problems as well as the accuracy achieved over diffusion peers are investigated there.

The rest of this article is organized as follows. In section 2, we propose the coupled SP_3-ACMFD approach adopted for reactor core static analysis. Section 3 is devoted to benchmark problems supporting the methodology described earlier. Therein, a number of reactor cores are studied at the static mode in detail. We finally sum up the work with a conclusion in section 4.

2. The SP_3-ACMFD technique applied for static solutions

The primary idea behind development of the SP_N approximation was to simplify the application of heavily coupled P_N equations in multidimensional space. The appraoch was successful in damping the number of coupled equations down to $N+1$ in a 3D SP_N system from $(N+1)^2$ for a full 3D P_N analysis ($N \in$ odd).

2.1. SP3 equations for angular approximation

Briefly, a SP_3 system of equations is presented through the following coupled system [16],

$$\begin{aligned}
&\nabla.\phi_{1g} + \Sigma_{rg}\phi_{0g} = S_{0g} = \sum_{g'\neq g}^{G} \Sigma_{sg'g}\phi_{0g'} + \frac{\chi_g}{k_{eff}} \sum_{g'=1}^{G} \nu\Sigma_{fg'}\phi_{0g'},\\
&\frac{2}{3}\nabla\phi_{2g} + \frac{1}{3}\nabla\phi_{0g} + \Sigma_{trg}\phi_{1g} = 0,\\
&\frac{3}{5}\nabla.\phi_{3g} + \frac{2}{5}\nabla.\phi_{1g} + \Sigma_{tg}\phi_{2g} = 0,\\
&\frac{3}{7}\nabla\phi_{2g} + \Sigma_{tg}\phi_{3g} = 0,
\end{aligned} \tag{1}$$

where all parameters have their conventional definitions used in the transport theory. Next, odd order moments are substituted by even moments obtained via rearrangement of equations. The result can be displayed in matrix form as [16].

$$\begin{bmatrix} -D_1\nabla^2 + \Sigma_r & -2\Sigma_r \\ -\frac{2}{3}\Sigma_r & -D_3\nabla^2 + \Sigma_{rt} \end{bmatrix}_g \cdot \begin{bmatrix} \Phi_0 \\ \phi_2 \end{bmatrix}_g = S_{0,g} \begin{bmatrix} 1 \\ -\frac{2}{3} \end{bmatrix}_g \tag{2}$$

where

$$\Phi_0 \equiv \phi_0 + 2\phi_2,\ \ \Sigma_{rt} \equiv \frac{5}{3}\Sigma_t + \frac{4}{3}\Sigma_r,\ \ D_1 \equiv \frac{1}{3\Sigma_{tr}},\ \ D_3 \equiv \frac{3}{7\Sigma_t}. \tag{3}$$

Partial currents can also be introduced as a special combination of moments of surface fluxes and moments of net currents

$$j_1^{\pm} = \frac{1}{4}\Phi_{0s} \pm \frac{1}{2}J_1 - \frac{3}{16}\phi_{2s},\ \ j_3^{\pm} = \frac{7}{16}\phi_{2s} \pm \frac{1}{2}J_3 - \frac{1}{16}\Phi_{0s}. \tag{4}$$

where current moments are defined as.

$$J_1 = -D_1\nabla\Phi_0,\ \ J_3 = -D_3\nabla\phi_2. \tag{5}$$

Theoretically, the solution of Eq. (2) determines the scalar flux (ϕ_0) plus related quantities. As typical for all nodal methods, in the first step Eq. (2) is integrated over the volume of node m and dimensions h_u $(u = x,y,z)$.

$$\begin{aligned}
&\sum_{u=x,y,z} \left[\left(J_{1,g,u}^{m_u+} - J_{1,g,u}^{m_u-} \right) \Big/ h_{u,m_u} \right] + \Sigma_{r,g}\overline{\Phi}_{0,g} - 2\Sigma_{r,g}\overline{\phi}_2 \\
&\quad - \sum_{\substack{g'=1 \\ g'\neq g}}^{G} \Sigma_{g'\to g}\left(\overline{\Phi}_{0,g'} - 2\overline{\phi}_{2,g'}\right) = \frac{\chi_g}{k_{eff}} \sum_{g'} \nu\Sigma_{fg'}\left(\overline{\Phi}_{0,g'} - 2\overline{\phi}_{2,g'}\right),\\
&\sum_{u=x,y,z} \left[\left(J_{3,g,u}^{m_u+} - J_{3,g,u}^{m_u-} \right) \Big/ h_{u,m_u} \right] + \Sigma_{rt,g}\overline{\phi}_{2,g} - \frac{2}{3}\Sigma_{r,g}\overline{\Phi}_{0,g} \\
&\quad + \frac{2}{3}\sum_{g'\neq g} \Sigma_{sg'g}\left(\overline{\Phi}_{0,g'} - 2\overline{\phi}_{2,g'}\right) = -\frac{2}{3}\left(\frac{\chi_g}{k_{eff}} \sum_{g'} \nu\Sigma_{fg'}\left(\overline{\Phi}_{0,g'} - 2\overline{\phi}_{2,g'}\right) \right).
\end{aligned} \tag{6}$$

Establishing a relation between the average nodal surface currents and the average nodal moments would lead to an eigenvalue system of equations for which the ACMFD framework is further invoked to solve the problem.

2.2. ACMFD method for spatial descretization

As quite conventional in nodal methods, three transverse integrations over the SP_3 equations have to be performed to generate three one dimensional equations with transverse leakage terms. The result would be three transverse integrated equations of the

form

$$\begin{bmatrix} -D_1\frac{d^2}{du^2}+\Sigma_r & -2\Sigma_r \\ -\frac{2}{3}\Sigma_r & -D_3\frac{d^2}{du^2}+\Sigma_{rt} \end{bmatrix}_g \begin{bmatrix} \Phi_0 \\ \phi_2 \end{bmatrix}_g = S_{0,g}\begin{bmatrix} 1 \\ -\frac{2}{3} \end{bmatrix} - \begin{bmatrix} L_1 \\ L_3 \end{bmatrix}_g \tag{7}$$

where $u = x$, y, or z and,

$$L_1(u) = \frac{1}{h_v\, h_w}\iint -D_1\left(\frac{\partial^2\Phi_0}{\partial v^2}+\frac{\partial^2\Phi_0}{\partial w^2}\right) dv\, dw\,; \qquad v, w = x, y, z\ (v\neq w\neq u). \tag{8}$$

A similar equation can also be derived for $L_3(u)$ in Eq. (7) by substituting proper parameters. Eq. (7) can be expressed in a condensed form as

$$\left(\frac{d^2}{du^2}-\mathrm{A}\right)|\varphi(u)\rangle = \mathrm{D}^{-1}|L(u)\rangle. \tag{9}$$

where $\mathbf{D}_u$ is a diagonal matrix containing D_{ig}, $|\varphi(u)\rangle = [\Phi_{0,g} \quad \phi_{2,g}]^{\mathrm{T}}$ and $\mathbf{A}$ is defined by

$$\mathrm{A} = \begin{bmatrix} \mathrm{A}^{11} & \mathrm{A}^{12} \\ \mathrm{A}^{21} & \mathrm{A}^{22} \end{bmatrix}_{2G\times 2G}, \quad \mathrm{A}^{ij} = \left[a^{ij}_{gg'}\right]_{G\times G},$$

$$a^{11}_{gg'} = \frac{1}{D_{1,g}}\begin{cases} \Sigma_{s,g'\to g}+\chi_g\nu\Sigma_{f,g'}\big/k_{eff} & g\neq g' \\ -\Sigma_{r,g}+\chi_g\nu\Sigma_{f,g}\big/k_{eff} & g=g' \end{cases},$$

$$a^{12}_{gg'} = \frac{-2}{D_{1,g}}\begin{cases} \Sigma_{s,g'\to g}+\chi_g\nu\Sigma_{f,g'}\big/k_{eff} & g\neq g' \\ -\Sigma_{r,g}+\chi_g\nu\Sigma_{f,g}\big/k_{eff} & g=g' \end{cases},$$

$$a^{21}_{gg'} = \frac{-2}{3D_{3,g}}\begin{cases} \Sigma_{s,g'\to g}+\chi_g\nu\Sigma_{f,g'}\big/k_{eff} & g\neq g' \\ 1.5\left(\Sigma_{r,g}-\chi_g\nu\Sigma_{f,g}\big/k_{eff}\right) & g=g' \end{cases},$$

$$a^{22}_{gg'} = \frac{4}{3D_{3,g}}\begin{cases} \Sigma_{s,g'\to g}+\chi_g\nu\Sigma_{f,g'}\big/k_{eff} & g\neq g' \\ -3\Sigma_{rt,g}/4+\chi_g\nu\Sigma_{f,g}\big/k_{eff} & g=g' \end{cases}. \tag{10}$$

In this paper the group transverse leakage for the typical node m is approximated by a quadratic polynomial as

$$L^{i,g}_m(u) = c^{i,g}_{0,m} + u\, c^{i,g}_{1,m} + \left(u^2-\frac{h^2_{u,m}}{12}\right)c^{i,g}_{2,m}\,; \quad i = 1, 3, \qquad g = 1, 2, \ldots, G. \tag{11}$$

with $h_{u,m}$ being the length of node m along the u direction. To find the expansion coefficients ($c^{i,g}_{n,m}$; n = 0, 1, 2), a curve fitting process is performed which establishes a relation among $c^{i,g}_{n,m}$ and the amounts of average transverse leakages over node m and its two adjacents i.e. m-1 and m+1 in the same direction (currently supposed to be known). Therefore, one can write

$$\begin{aligned} \bar{L}^{m-1}_u &= \frac{1}{h_{u,m-1}}\int_{-\frac{h_{u,m}}{2}-h_{u,m-1}}^{-\frac{h_{u,m}}{2}} L_{i,g}(u)du = \\ & c^i_{0,m} - (h_{u,m-1}+h_{u,m})c^i_{1,m}\big/2 \\ & + (h_{u,m-1}+h_{u,m})(2h_{u,m-1}+h_{u,m})c^i_{2,m}\big/6; \\ \bar{L}^{m}_u &= \frac{1}{h_{u,m}}\int_{-\frac{h_{u,m}}{2}}^{+\frac{h_{u,m}}{2}} L_{i,g}(u)du = c^i_{0,m}; \\ \bar{L}^{m+1}_u &= \frac{1}{h_{u,m+1}}\int_{+\frac{h_{u,m}}{2}}^{+\frac{h_{u,m}}{2}+h_{u,m+1}} L_{i,g}(u)du = \\ & c^i_{0,m} + (h_{u,m+1}+h_{u,m})c^i_{1,m}\big/2 \\ & + (h_{u,m+1}+h_{u,m})(2h_{u,m+1}+h_{u,m})c^i_{2,m}\big/6; \\ & u = x, y, z; \end{aligned} \tag{12}$$

where $\bar{L}_u$ for nodes m-1, m and m+1 are obtained through a straightforward 1D integration over the volume of each node leading to an algebraic summation of average transverse currents over the node boarders. As a result, the unknown $|L(u)\rangle$ in Eq. (9) can be presented as a function of transverse currents which is assumed to be known thanks to the previous iterations during the iterative solution or an implicit approach, as an alternate solution strategy. Therefore, $|L(u)\rangle$ in Eq. (9) is now supposed to be known and the dependency of lateral directions was removed.

Despite achievments in spatial simplicities, Eq. (9) still suffers from extensive group and moment couplings which must be resolved to enjoy the ACMFD with analytic solution. By benefiting the diagonalization procedure, the 2 × G system of coupled equations could be reduced into a set of 2 × G uncoupled equations. To this end, as performed by Lozano et al. [21] for the diffusion case, we can define some conversion matrices to shift over the so-called *modal* space wherein the equations could get decoupled. Using the matrix algebra we may have

$$\begin{aligned} & \mathrm{A}|v_m\rangle = \lambda_m|v_m\rangle\ ;\ m = 1, \ldots, 2G.\ \mathrm{R}^{-1} = [\\ & \times |v_1\rangle\ \ |v_2\rangle\ \ldots\ |v_{2G}\rangle];\ \mathrm{RAR}^{-1} = \lambda, \end{aligned} \tag{13}$$

where $|v_m\rangle$ represents the eigenvector of $\mathbf{A}$, and λ is a diagonal matrix for eigenvalues of $\mathbf{A}$. Nodal vectors could be transferred into the modal spaces through the conversion matrices as

$$|\psi(u)\rangle = \mathrm{R}|\varphi(u)\rangle,\ \ |\ell(u)\rangle = \mathrm{RD}^{-1}|L(u)\rangle \tag{14}$$

and inverse transforms could be used for modal to nodal shift. Using transforms given by (14), Eq. (9) can be represented in the modal space as

$$\frac{d^2\psi_m(u)}{du^2} - \mu_m\psi_m(u) = \ell_m(u); \quad m = 1, .., M, \qquad u = x, y, z \tag{15}$$

with the following solution:

$$\psi_m(u) = P_m(u) + A_{m,u}e^{+\sqrt{\mu_m}u} + B_{m,u}e^{-\sqrt{\mu_m}u} \tag{16}$$

where $P_m(u)$ is the particular solution corresponding to the specific force term $\ell_m(u)$ at the *rhs* of Eq. (15), and $A_{m,u}$ and $B_{m,u}$ are two constants obtained with the help of boundary conditions. The general modal solution derived in Eq. (16) could be specialized for a particular 1D node expanded from u=-h/2 to u=+h/2. In this regard, some mathematical manipulation ends to a relation among the mean modal flux over the node, modal currents and flux moments on the node borders as

$$\begin{aligned}\psi_m\left(\pm\frac{h_u}{2}\right) &= P_m\left(\pm\frac{h_u}{2}\right) + \xi^f_{m,u}\left[\overline{\psi}_m - \overline{P}_m\right] \\ &\pm\frac{h_u}{2}\xi^j_{m,u}\frac{d}{du}\left[\psi_m\left(\pm\frac{h_u}{2}\right) - P_m\left(\pm\frac{h_u}{2}\right)\right] \\ m &= 1,..,M, \quad u = x,y,z\end{aligned} \tag{17}$$

where

$$\xi^f_{m,u} \equiv \frac{\sqrt{\mu_m}h_u}{\sinh(\sqrt{\mu_m}h_u)}, \quad \xi^j_{m,u} \equiv \frac{\tanh(\sqrt{\mu_m}h_u/2)}{\sqrt{\mu_m}h_u/2} \tag{18}$$

are defined for simplicity. Now, noting Eq. (9), the decoupled equations stated by Eq. (17) are transferred back into the nodal space to have a system of coupled equations there. The coupled nodal system can now be represented as

$$\begin{aligned}\left|\varphi_u\left(\pm\frac{h_u}{2}\right)\right\rangle &= \Gamma^f_u|\overline{\varphi}\rangle \mp \frac{h_u}{2}\Gamma^j_u \mathrm{D}^{-1}\left|J_u\left(\pm\frac{h_u}{2}\right)\right\rangle - \mathrm{R}^{-1}\left|\Theta\left(\pm\frac{h_u}{2}\right)\right\rangle \\ u &= x,y,z\end{aligned} \tag{19}$$

where $\left|\Theta\left(\pm\frac{h_u}{2}\right)\right\rangle$ is the vector of $\theta_{m,u}\left(\pm\frac{h_u}{2}\right)$ elements for m = 1,2, …,2G as

$$\theta_{m,u}\left(\pm\frac{h_u}{2}\right) = \xi^f_{m,u}\overline{P}_{m.u} - P_{m,u}\left(\pm\frac{h_u}{2}\right) \pm \frac{h_u}{2}\xi^j_{m,u}\frac{d}{du}P_{m,u}\left(\pm\frac{h_u}{2}\right) \tag{20}$$

and

$$\Gamma^f_u = R^{-1}\Xi^f_u R, \quad \Gamma^j_u = R^{-1}\Xi^j_u R \tag{21}$$

are two coefficient matrices wherein Ξ denote diagonal matrices for ξs. Imposing continuity conditions for the moments and currents at the interfaces of samples nodes m-1 and m establishes a relation between $\left|\bar{J}^{m_u}_{u,L}\right\rangle$ and $|\overline{\varphi}_u\rangle$ for the two nodes as

$$\begin{aligned}\left|\bar{J}^{m_u}_{u,L}\right\rangle &= \frac{1}{2}\left(h_u^{m_u-1}\Gamma_u^{j,m_u-1}\left[\mathrm{D}^{m_u-1}\right]^{-1} + h_u^{m_u}\Gamma_u^{j,m_u}\left[\mathrm{D}^{m_u}\right]^{-1}\right)^{-1} \\ &\left(\Gamma_u^{f,m_u-1}\left|\overline{\varphi}^{m_u-1}\right\rangle - \left[\mathrm{R}^{m_u-1}\right]^{-1}\left|\Theta^{m_u-1}_{u,R}\right\rangle - \Gamma_u^{f,m_u}|\overline{\varphi}^{m_u}\rangle\right. \\ &\left.+\left[\mathrm{R}^{m_u}\right]^{-1}\left|\Theta^{m_u}_{u,L}\right\rangle\right), \; u = x,y,z; \quad L: \textit{left}, \quad R: \textit{right}\end{aligned} \tag{22}$$

Finally, to characterize the equations, two external boundary conditions must be further incorporated. For the node M subjected to a reflective surface the current $\left|\bar{J}^{M}_{u}\right\rangle$ damps to zero at the boundary, and for the node M' with free surface, the net partial incoming current in Eq. (4) vanishes by force. This is performed through setting

$$\begin{aligned}&\left|J^{M'}_u\left(\pm\frac{h_{u,FS}}{2}\right)\right\rangle = \pm\mathrm{B}\left|\varphi^{M'}_u\left(\pm\frac{h_{u,FS}}{2}\right)\right\rangle, \; B = \frac{1}{8}\begin{bmatrix}4 & -3\\ -1 & 7\end{bmatrix}, \quad FS \\ &: \text{Free Surface}.\end{aligned} \tag{23}$$

for all energy groups of node M' where "+" goes for the right free surface while "−" comes with the left free surface.

Finally, substituting the terms of currents stated by Eq. (22) for different $J^{m_u\pm}_{i,g,u}$ terms into the nodal balance Eq. (6) plus incorporating external boundary conditions, renders a multigroup eigenvalue system of the form $\mathbf{M}|\overline{\varphi}\rangle = \frac{1}{k_{eff}}\mathbf{F}|\overline{\varphi}\rangle$ for the static state. The commonly invoked power iteration can in general solve the problem straightforwardly with transverse leakage updating included. Fig. 1 presents a calculation flow for the solution of equations described earlier.

3. Numerical results

Based on the theory, a code named SIMANOD is developed in F90 to perform 3D multigroup static solutions benefiting the SP_3-ACMFD scheme. The engine was also boosted by the Math Kernel Library (MKL). The powerful GMRES solver is invoked to solve the final linear system of the equations.

Four benchmark problems are chosen for the evaluation of static results. According to the theory, we expect superior outcome compared to the diffusion predition especially in problems with high heterogenuity. To prove it, we have further developed a code called DIFANOD based on the ACMFD but for the difussion analysis. On the other hand, the theory states that the SP_3 should result in inferoir results than the transport solutions of course with lower costs. For complex problems however, the privilege balances toward the interim approaches (SP_3 included) as the solution costs must not exceed a logical threshold. Compartive outcomes could be traced in the supplied static benchmarks. The convergence criteria for k_{eff} and the local flux are 10^{-7} and 10^{-4} respectively for all tests.

3.1. Test Case I: a small homogeneous cube

As the first, we consider a simple homogeneous cube of 10 cm in each side. The cube dimension is small enough to observe cosiderable anisotropy of the neutron flux as a result of high boundary to volume ratio. Geometry of the problem is demonstrated in Fig. 2 wherein a few boundary nodes are also specified. Also, one group cross sections are $(\Sigma_t, \nu\Sigma_f, \Sigma_s) = (1, 0.88, 0.25)\ \mathrm{cm}^{-1}$. Cubic nodes of unit volume fill the cube for both SIMANOD and DIFANOD.

As the reference, MCNPX [22] results for the k_{eff} is reported with 1 pcm standard deviation, and the maximum relative standard deviation for the fluxes is 0.0006.

In Eq. (24) we have introduced the Relative Power Density (RPD) for node i which is applicable for the comparison of power distibution. In fact, RPD^i is the ratio of power density in node i to mean power density of the core.

$$\mathrm{RPD}^i = \frac{\sum_{g=1}^{G}\Sigma^i_{f,g}\overline{\phi}^i_{0,g}}{\left(\sum_{i=1}^{N}V^i\sum_{g=1}^{G}\Sigma^i_{f,g}\overline{\phi}^i_{0,g}\right)\Big/\left(\sum_{i=1}^{N}\lambda^i V^i\right)},$$

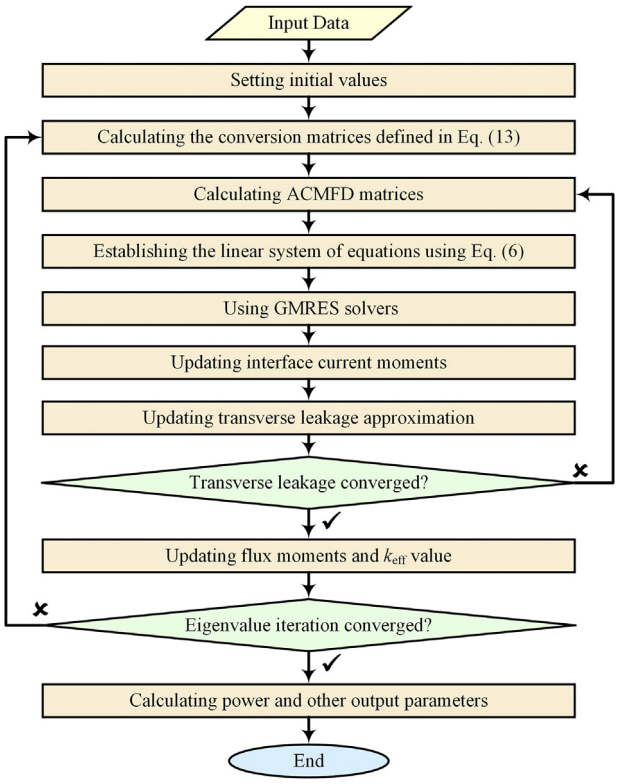

Fig. 1. A calculation flow diagram for the static SP_3-ACMFD approach.

$$\lambda^i = \begin{cases} 1\,; & \Sigma^i_{f,g} \neq 0 \\ 0\,; & \Sigma^i_{f,g} = 0 \end{cases}. \tag{24}$$

Table 1 demonstarates that switching from DIFANOD to SIMANOD i.e. diffusion to SP_3 improves the error in the effective multiplication factor from −543 to +43 pcm. Also in Table 1, the improvement is quite sensible (nearly 8 times) in the average of absolute errors in RPD over the whole core. By moving from the cube center to the wall, the flux anisotropy is intensified and consequently the need for finer angular resolution is much felt. To understand the maximum improvement obtained by SIMANOD against DIFANOD, the RPD is monitored over the boundary nodes depicted in Fig. 2. As expected, corner nodes pose the maximum error due to the high flux gradient there. Via Fig. 3, one can confirm that the approach adopted in SIMANOD nearly halves the absolute error of this node compared to that of DIFANOD.

3.2. Test Case II: a 2D LWR with UOX-MOX fuels (C5G2)

To illustrate the capabilities of the developed codes in analyzing the MOX fuel cores, this two-dimensional two-group problem is studied in detail. Capilla et al. [23] introduced the problem as a simplified version of the famous C5G7 core originally proposed in Ref. [24]. The core configuration is depicted in Fig. 4 and the two-group constants of the problem can be found in Ref. [23]. Each assembly must be divided into at least 17 × 17 rectangles with the minimum of 1156 nodes in the active core. Nodes of variable size however could be employed for the surrounding homogeneous reflector.

To assess the proposed approach over this highly heterogeneous benchmark, the minimum number of required nodes are used for discretizing the core. Also, to improve the resolution for the

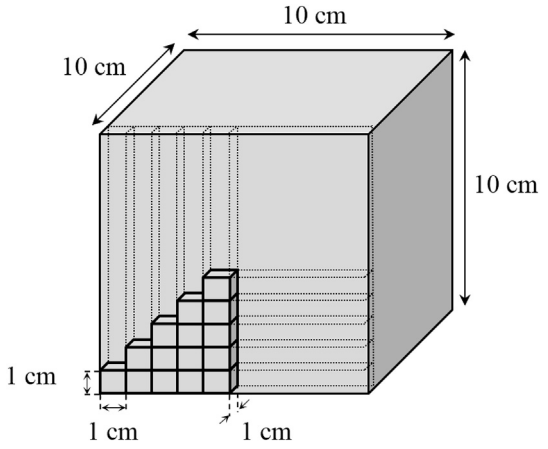

Fig. 2. Geometry of the simple homogeneous cube (Test Case I).

Table 1
Eigenvalue search results for the simple homogeneous cube (Test Case I).

CODE	k_{eff}	ε_k [a] [pcm]	ε_{ave} [b] [%]	ε_{max} [b] [%]
MCNPX (ref.)	1.06938	0	0	0
SIMANOD	1.06981	+43	0.22	1.99
DIFANOD	1.06395	−543	1.76	4.62

[a] ε_k is the error in effective multiplication factor in comparison with the reference value (pcm).
[b] ε_{ave} and ε_{max} are average and maximum of the absolute percentage of relative errors in nodal power densities.

thermal group, nodes of the same size are tiled over the water reflector. As a result the problem comprises 2601 nodes in sum. Reference solution of the benchmark is generated by MCNPX to facilitate a detail comparison for pin powers as well as the eigenvalue. Again, MCNPX results for the k_{eff} is reported with 1 pcm standard deviation, and the maximum relative standard deviations for pinwise fluxes are 0.0006 and 0.0008 for the fast and thermal energy groups, respectively. Eigenvalue search results plus calculated errors are reported in Table 2. Moreover, to see the improvement obtained over the diffusion approximation results by the DIFANOD are also reported there. Absolute values of pin power distribution error over the assemblies are further compared in Fig. 5.

Table 2 displays a relatively low-cost switch from the commonly invoked diffusion method to the SP_3 approach which deserves a reduction in the error of k_{eff} from 90 to 31 pcm (nearly 3 times lower). The gain in pin powers are also brilliant. The maximum error of pin powers is reduced by a factor of 5 while in average, the

MCNPX (Reference) SIMANOD Err. [%] DIFANOD Err. [%]				0.8423 0.28 2.54
			0.7184 0.33 2.51	0.7782 0.27 2.49
		0.5081 0.35 2.37	0.6042 0.33 2.43	0.6540 0.35 2.49
	0.2740 0.16 2.12	0.3728 0.33 2.33	0.4432 0.33 2.42	0.4798 0.33 2.47
0.0841 **-1.99** **4.62**	0.1509 -0.53 3.93	0.2049 -0.21 4.35	0.2435 -0.17 4.49	0.2636 -0.16 4.56

Fig. 3. RPD results for the boundary nodes shown in Fig. 2 (Test Case I).

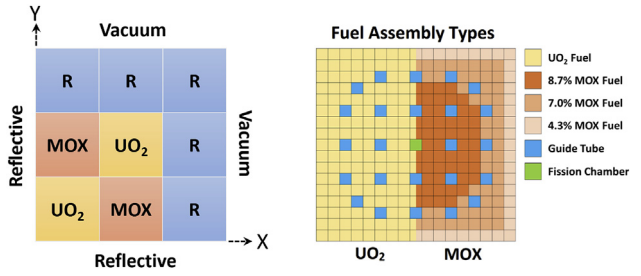

Fig. 4. Geometry of the C5G2 benchmark (Test Case II).

Table 2
Eigenvalue search results for the C5G2 benchmark (Test Case II).

Code	k_{eff}	ε_k[pcm]	ε_{ave}[%]	$\varepsilon_{\max}$[%]
MCNPX	0.97050	0	0	0
SIMANOD	0.97081	+31	0.13	0.56
DIFANOD	0.97140	+90	0.49	2.95

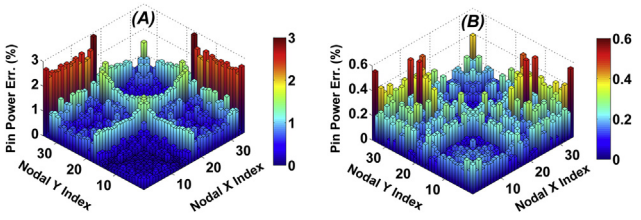

Fig. 5. Pin power errors in the C5G2 benchmark using (A) DIFANOD, and (B) SIMANOD (Test Case II).

errors are at least dropped by a factor of 3. The map of pin power errors are further illustrated in Fig. 5 where as demonstrated, maximum errors are appeared near the borders.

3.3. Test Case III: the modified IAEA-3D problem

As a 3D test, the simplified IAEA's PWR is investigated to assess the performance of SIMANOD under normal operation. The problem was first introduced by Hébert [3] who modified the original core proposed in Ref. [25]. The core specification and the two group constants are the same as those reported in Ref. [3].

Cho et al. [26] modeled the problem using the code DANTSYS with S_{16} approximation which is taken as reference. For our purpose, we axially subdivided each assembly into 19 nodes ($1 \times 1 \times 19$) to obtain the results. The multiplication factor and the relative powers of the assemblies are compared against the reference results in Table 3 and Fig. 6 respectively. Again, a substantial improvement comes along the expectations when shifting over the SP_3 equations. As seen in Table 3, the eigenvalue error comes down to 2 pcm from 48 pcm, and both ε_{ave} and $\varepsilon_{\max}$ experience an improvement by a factor of nearly four. Note that the power errors in Table 3 are defined over assemblies. Meanwhile, Bahabadi et al. [7] have supposed 76 ($2 \times 2 \times 19$) nodes per assembly for a SP_3-AFEN analysis using their MGANSP3 code. Results are very close to those we obtained but in comparison, the absolute error in k_{eff} and the maximum error in relative powers decrease by 14 pcm and 0.77%, respectively.

Table 3
Eigenvalue search results for the modified IAEA-3D problem (Test Case III).

Method	k_{eff}	ε_k	ε_{ave}	$\varepsilon_{\max}$
DANTSYS (S16)	1.02956	–	–	–
SIMANOD	1.02958	2	0.19	0.68
DIFANOD	1.02908	48	0.72	2.91

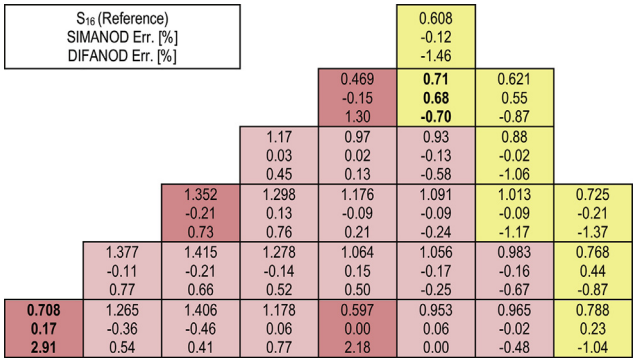

Fig. 6. Relative power of the assemblies for the modified IAEA-3D problem (Test Case III).

3.4. Test Case IV: Takeda's small fast breeder reactor

As the last problem, a small fast breeder reactor (FBR-SQ) is chosen among famous benchmark problems of Takeda and Ikeda [27]. Two different cases of the problem are considered: (*i*) *uncontrolled,* where control channel is filled by the sodium coolant, and (*ii*) *partially controlled*, where the control rod is half inserted. The reference results are adopted from the work of Ryu and Joo [28] who employed the Monte Carlo code McCARD. The size of nodes in both SIMANOD and DIFANOD, are assumed $5 \times 5 \times 5$ cm^3. Table 4 lists a comparison among evaluated parameters. Also, relative power distributions of cases *i* and *ii* are compared in Fig. 7 for core region. Four group nodal fluxes of the core's fifth layer (from the top) are depicted in Fig. 8. The flux is normalized such that the neutron generation rate equals unity over the full core.

Overall, inspection of Table 4 reveals that the error of proposed method lies in the acceptable range for both conditions, and for the partially controlled case, the eigenvalue errors are generally more for uncontrolled state, as expected. The maximum error however remains unchanged for SIMANOD. It is also observed that the eigenvalue errors are reduced by an order of magnitude when switching from SIMANOD to DIFANOD beside a considerable reduction in the mean values of power errors. The only drawback is the maximum error of power in uncontrolled case which goes up by 0.08%.

Over the detailed comparisons given in Fig. 7, one should note that the reference values of McCARD have been reported only with fixed 3 digits after point. Therefore, numerical comparisons made in Fig. 7 may not be entirely true especially inside the blanket where the number of reference meaningful digits may be reduced down to one. That's why we have only reported the maximum relative error in power for the core region.

Table 4
Eigenvalue search results for Takeda's small fast breeder reactor benchmark (Test Case IV).

Code	Case	k_{eff}	ε_k[pcm]	ε_{ave}[a] [%]	$\varepsilon_{\max}$[a] [%]
McCARD (Ref.)	Uncontrolled	0.97370	0	0	0
Ryu and Joo [28]	Partially controlled	0.95967	0	0	0
SIMANOD	Uncontrolled	0.97342	−28	0.09	0.56
	Partially controlled	0.95926	−41	0.14	0.56
DIFANOD	Uncontrolled	0.96887	−480	0.27	0.48
	Partially controlled	0.95409	−558	0.28	0.75

[a] Errors are considered only in the core region.

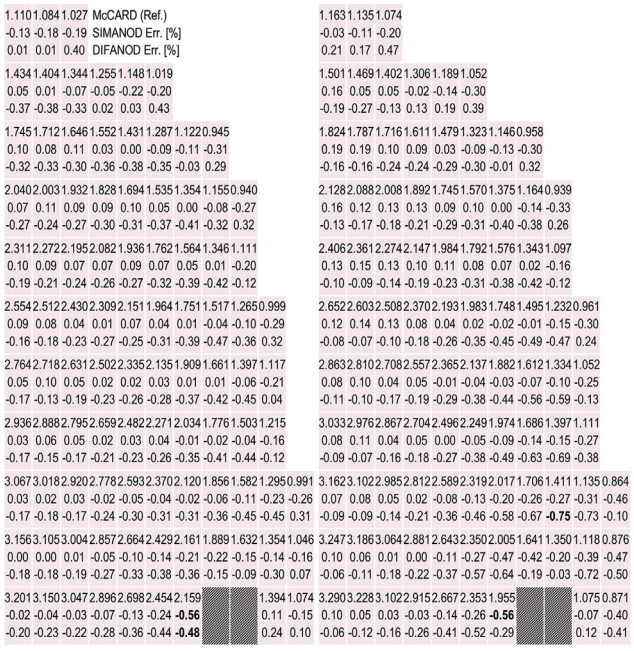

Fig. 7. Power distribution for Takeda's small fast breeder reactor benchmark, cases *i* and *ii* (Test Case IV).

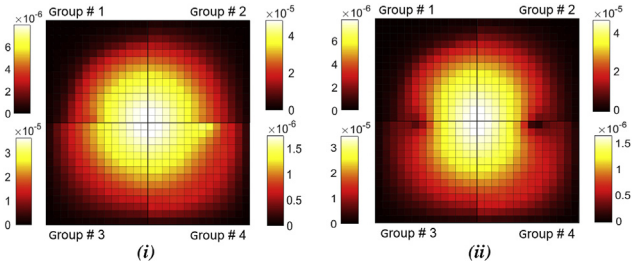

Fig. 8. Four-group scalar flux distribution for Takeda's small fast breeder reactor benchmark, cases *i* and *ii* (Test Case IV).

4. Conclusion

A coupled SP_3-ACMFD technique was proposed for reactor core analysis. The main privilege of the idea is the admissible accuracy compared to the diffusion approximation while less burden in comparison with P_3 resolution. To validate the idea a code called SIMANOD was developed for the static analysis of reactors with rectangular geometry. The approach proved robust for handling regular multigroup calculations. Simulations confirm that while the method is generally superior to the diffusion theory (DIFANOD), the overall accuracy is comparable with full transport approach. Static analyses suggest that the methodology can hopefully serve as an efficient platform for a further extension of the work to time dependent problems; an idea to be probed in Part II.

Acknowledgements

The authors wish to acknowledge the respectful reviewers for the thought out comments and suggestions over the work. We also highly gratitude Dr. T. Agahi for her invaluable cooperation in preparing the manuscript. Finally, technical supports by the Advanced Nuclear Computing Center (ANCC) are highly appreciated.

Appendix A. Supplementary data

Supplementary data to this article can be found online at https://doi.org/10.1016/j.net.2019.07.022.

References

[1] S.A. Thompson, Advanced Reactor Physics Methods for Heterogeneous Reactor Cores, The pennsylvania state university college of engineering, 2014.
[2] A. Henry, Nuclear-Reactor Analysis, second ed., MIT Press, 1980.
[3] A. Hébert, Mixed-dual implementations of the simplified Pn method, Ann. Nucl. Energy 37 (2010) 498–511.
[4] P. Kotiluoto, Adaptive Tree Multigrids and Simplified Spherical Harmonics Approximation in Deterministic Neutral and Charged Particle Transport, VTT Publications, 2007.
[5] G. Longoni, A. Haghighat, The even-parity simplified S_N equations applied to a MOX fuel assembly benchmark problem on distributed memory environments. PHYSOR 2004-the physics of fuel cycles and advanced nuclear systems, Global Developments (2004) 25–29.
[6] C. Beckert, U. Grundmann, Development and verification of a nodal approach for solving the multigroup SP3 equations, Ann. Nucl. Energy 35 (2008) 75–86.
[7] M.H.J. Bahabadi, A. Pazirandeh, M. Athari, New analytic function expansion nodal (AFEN) method for solving multigroup neutron simplified P_3 (SP_3) equations, Ann. Nucl. Energy 77 (2015) 148–160.
[8] A. Vidal-Ferràndiz, S. González-Pintor, D. Ginestar, C. Demazière, G. Verdú, Pin-wise homogenization for SPN neutron transport approximation using the finite element method, J. Comput. Appl. Math. 330 (2017) 806–821.
[9] Y.-A. Chao, A new and rigorous SP_N theory—Part III: a succinct summary of the GSP_N theory, the P_3 equivalent and implementation issues, Ann. Nucl. Energy 119 (2018) 310–321.
[10] Y.-A. Chao, A new and rigorous SP_N theory for piecewise homogeneous regions, Ann. Nucl. Energy 96 (2016) 112–125.
[11] Y.-A. Chao, A new and rigorous SP_N theory—Part II: generalization to GSP_N, Ann. Nucl. Energy 110 (2017) 1176–1196.
[12] A. Cherezov, R. Sanchez, H.G. Joo, A reduced-basis element method for pin-by-pin reactor core calculations in diffusion and SP_3 approximations, Ann. Nucl. Energy 116 (2018) 195–209.
[13] C. Zhang, G. Chen, Fast solution of neutron transport SP_3 equation by reduced basis finite element method, Ann. Nucl. Energy 120 (2018) 707–714.
[14] T.-Y. Lin, Y.-W.H. Liu, A next generation method for light water reactor core analysis by using global/local iteration method with SP_3, Ann. Nucl. Energy 118 (2018) 49–60.
[15] W. Yang, H. Wu, Y. Li, L. Cao, S. Wang, Acceleration of the exponential function expansion nodal SP3 method by multi-group GMRES algorithm for PWR pin-by-pin calculation, Ann. Nucl. Energy 120 (2018) 869–879.
[16] T. Downar, D. Lee, Y. Xu, T. Kozlowski, User and Theory Manual for the PARCS Neutronics Core Simulator (U.S. NRC Core Neutronics Simulator), School of Nuclear Engineering Purdue University, 2004.
[17] M. Tatsumi, A. Yamamoto, Advanced PWR core calculation based on multi-group nodal-transport method in three-dimensional pin-by-pin geometry, J. Nucl. Sci. Technol. 40 (2003) 376–387.
[18] T. Bahadir, S. Lindahl, S.P. Palmtag, SIMULATE-4 multi-group nodal code with microscopic depletion model, in: American Nuclear Society Topical Meeting in Mathematics and Computations, Avignon, France, 2005.
[19] Y.A. Chao, A Theoretical Analysis of the Coarse Mesh Finite Fifference Representation in Advanced Nodal Methods. Mathematics and Computation, Reactor Physics and Environmental Analysis in Nuclear Applications, Senda Ed., 1999, pp. 117–126. Madrid.
[20] J.M. Aragonés, C. Ahnert, N. García-Herranz, The analytic coarse mesh finite difference method for multigroup and multidimensional diffusion calculations, Nucl. Sci. Eng. 157 (2007) 1–15.
[21] J.-A. Lozano, N. García-Herranz, C. Ahnert, J.-M. Aragonés, The analytic nodal diffusion solver ANDES in multigroups for 3D rectangular geometry: development and performance analysis, Ann. Nucl. Energy 35 (2008) 2365–2374.
[22] M.U.s. Manual, Version 2.7. 0, Los Alamos National Laboratory, Los Alamos (NM), 2011.
[23] M. Capilla, D. Ginestar, G. Verdú, Applications of the multidimensional P_L equations to complex fuel assembly problems, Ann. Nucl. Energy 36 (2009) 1624–1634.
[24] OECD/NEA, Benchmark on Deterministic Transport Calculations without Spatial Homogenisation: a 2-D/3-D MOX Fuel Assembly Benchmark. NEA/NSA/DOC(2003)16, 2003.
[25] Argonne Code Center, ANL Benchmark Book-Report ANL-7416, Argonne National Laboratory, Argonne, IL, 1977.
[26] B. Cho, J.H. Won, N.Z. Cho, Analytic function expansion nodal(AFEN) method extended to multigroup simplified P_3 (SP3) equations via partial current moment transformation, Trans. Am. Nucl. Soc. 103 (2011) 714–717.
[27] T. Takeda, H. Ikeda, 3-D neutron transport benchmarks, J. Nucl. Sci. Technol. 28 (1991) 656–669.
[28] E.H. Ryu, H.G. Joo, Finite element method solution of the simplified P_3 equations for general geometry applications, Ann. Nucl. Energy 56 (2013) 194–207.